Feasibility of NIR tomographic reconstruction with multispectral continuous wave data by mapping into frequency domain data

Heng Xu[1*], Brian W. Pogue[1 #], Hamid Dehghani[1], Roger Springett[2], Keith D. Paulsen[1], Jeff F. Dunn[2]
[1]Thayer School of Engineering, Dartmouth College, Hanover NH 03755
[2]Department of Diagnostic Radiology, Dartmouth Medical School, Hanover NH 03755.

ABSTRACT

Diffuse near-infrared tomography of tissue can provide intrinsically useful information about total hemoglobin, oxygen saturation, water and cytochromes within tissue, yet to extract this information spectral data is required at many wavelengths. In this study, we examine a new approach to using multispectral continuous wave measurements through tissue along with second-derivative data analysis methods to estimate the pathlength in tissues over multiple tomographic paths. The goal of this work has been to demonstrate that the optical differential pathlength that is estimated by spectroscopy methods is directly related to the optical pathlength as measured by frequency-domain signals. This direct relation then allows the use of tomographic algorithms which have been developed for frequency-domain optical tomography to be applied to multispectral continuous wave data. The theoretical development is presented here, along with numerical validation in homogeneous and heterogeneous tissue-simulating regions. These results indicate that the approach outlined is valid and provides the theoretical basis for developing multispectral near-infrared tomography of tissues.

1. INTRODUCTION

Near infrared spectroscopy [1, 2] has been used as a non-invasive approach to study mammalian tissues for almost twenty years. The relative low absorption of tissues in this wavelength range makes it possible for photons to travel a considerable depth and pick up the features of some important tissue chromophores, such as hemoglobin, cytochrome oxidize and water. These features directly indicate tissue metabolism which is essential to monitor functional changes or detect diseases in a variety of applications. [3-6] In the early studies, most of near infrared spectroscopy systems made intensity measurements at several discrete wavelengths and used the modified Beer-Lambert law to calculate changes in chromophore concentrations. The modified Beer-Lambert law assumes the optical pathlength is a greater than the optode spacing due to the multiple scattering by the tissue and accurate estimation of this pathlength is essential so that chromophore changes can be expressed in units of concentration. [11, 12]The optical pathlength is usually called the differential pathlength and has been shown mathematically to be equal to the intensity weighted mean pathlength. Measurement of this pathlength is therefore very critical in such studies and is also very important to other imaging applications. In this study, a new method to qualify mean pathlength is used and tested for validity in tomography of tissue.

In order to measure the mean pathlength as well as the transmitted light intensity, [7-10]two methods have been widely accepted. One is the time domain system, which uses picoseconds laser pulse and ultra fast detectors to record the response of biological tissues and then calculate the mean flight time and hence pathlength. The other is the frequency domain system, which is the Fourier transformation of the time-domain system and employs radiofrequency (RF) modulated laser sources and takes both intensity and phase shift measurements of transmitted light. With both systems, it is necessary to use a model to quantify the optical absorption and scattering properties of tissues. [13-16]Both time domain system and frequency domain system typically use the diffusion approximation equation to model light transport in scattering dominated medium that makes it possible to reconstruct tomographic images using numerical methods, such as the finite element method (FEM). [17] Moreover, by applying laser sources at several wavelengths, chromophore concentrations can be calculated using the known specific absorption of the chromophores.

[18] Matcher et al have described a method to measure DP solely by a CCD full spectral system using second differential

* Heng.Xu@dartmouth.edu, Tel 1 (603) 650-1624, Fax 1 (603) 646-3856
# Pogue@dartmouth.edu, Tel 1 (603) 646-3861, Fax 1 (603) 646-3856

spectroscopy fitting. The essence of the method is to use the water absorption features in the wavelength range 650nm – 1040nm to calculate DP with an estimate of the water concentration. This type of CCD full spectral system takes a full spectrum over a large wavelength range, so it is more flexible to macroscopically capture chromophore absorption features than time domain system and frequency domain system which are limited by the choice of laser sources. However, on the other hand, it is challenging to quantify tissue with structural details due to the many wavelengths involved. Although topography is often used in spectroscopy systems, we haven't seen any trials to reconstruct tomographic images with spectroscopy systems.

At Dartmouth both frequency domain system and CCD full spectral system have been developed. [17, 19] The frequency domain system has shown promising success in breast cancer application. Both the diffusion approximation model and FEM method have been implemented successfully to solve the problem of light transport in scattering dominated tissues. The full spectral system which has limited photon detection ability is designed for smaller geometry applications such as rat cerebral studies. [20, 21] Our earlier studies have shown the success of imaging optical properties of rat head by frequency domain system with a priori information provided by MRI machine. The present goal is to obtain tomographic images as well with our full spectral system. Since full spectral system is able to estimate the DP and DP is equivalent to phase shift measured by frequency domain system, an intuitive question comes out, "Can we map CCD full spectral system measurements into frequency domain system to provide a means to fit for absorption coefficients and scattering coefficients with our current frequency domain system FEM approach?" This forms the hypothesis which will be tested in this study.

[12] Arridge et al have demonstrated the difference of intensity at 100 MHz and zero frequency was very small, which implies that the attenuation obtained in full spectral system is equivalent to the intensity in frequency domain system. If we could match the DP estimated in full spectral system to DP calculated from phase shift in frequency domain system, we are therefore able to implement the image reconstruction method of frequency domain system to full spectral system. (To make the expression simpler, we named the DP estimated in full spectral system as DPW and the DP calculated from phase shift in frequency domain system as DPP.) Keeping this goal in the mind, we will discuss the method to obtain DPW in full spectral system, how the DPW agrees and disagrees with DPP in different circumstances and propose a strategy to solve the disagreement.

2. METHODS

2.1 Estimate the differential pathlength in a homogeneous medium

In this section, we will introduce the method we use to get an estimate of the differential pathlength (DPW) in a homogeneous medium with our full spectral system, especially focusing on the mathematical model and assumptions and approximations we make during the process. [22] Although this method inherits the method that has been discussed by Matcher et al, some modifications have been made and therefore it is necessary to address the method in detail here. In non-scattering media, the relationship between the concentration of absorbing chromophores and attenuation can be modeled by a standard Beer Lambert law that states that the attenuation (A) is proportional to the product of the molar extinction coefficient, the chromophore concentration (C) and the optical pathlength (P). In a strongly scattering medium such as tissue, this simple expression does not hold because the light takes multiple paths between transmit and receive optodes so that there is no single optical pathlength. [18, 23] Many people, like Matcher et al, Kohl et al, typically used a modified Beer-Lambert law (Eq. 1) to address the scattering effect on the attenuation.

$$A = \gamma \mu_a l + G \tag{1}$$

Here A is the attenuation, l is the optode spacing and G is a term to describe the scattering losses. The term γ describes the effect of the mean pathlength of photons being increased by multiple scattering, which is conventionally termed the differential pathlength factor (DPF). The product of γ and l is the differential pathlength. Within the framework of the modified Beer-Lambert law, the attenuation is linear with respect to μ_a though, in reality, both γ and G are function of μ_a and μ_s. Matcher et al have described how to use second-differential analysis based on the modified Beer Lambert law together with the water concentration knowledge to provide an estimate of differential pathlength. Although we inherited their method, we use a mathematically more rigorous derivation where the assumptions are more transparent and easier to examine. We start our approach from the direct mathematical expansion of attenuation $A(\mu_a, \mu_s) = -\ln(I / I_0)$, where I is the intensity.

$$\Delta A \approx \frac{\partial A}{\partial \mu_a}\Delta\mu_a + \frac{\partial A}{\partial \mu_s}\Delta\mu_s \tag{2}$$

This approximation only holds when $\Delta\mu_a$ and $\Delta\mu_s$ are small. In general it is assumed that $\Delta\mu_s$ is zero in which case this equation resembles the modified Beer Lambert Law. Therefore, the measured change of attenuation is the product of a small change of absorption and differential pathlength (DP). Because the attenuation is determined by the optical properties ($\mu_a(\lambda), \mu_s(\lambda)$) and both of absorption and scattering coefficients are wavelength dependent, so the attenuation also is wavelength dependent. For the second differential analysis, we can expand $A(\mu_a(\lambda), \mu_s(\lambda))$ with respect to λ as:

$$\frac{\partial^2 A}{\partial \lambda^2} = \frac{\partial A}{\partial \mu_a}\frac{\partial^2 \mu_a}{\partial \lambda^2} + \frac{\partial^2 A}{\partial {\mu_a}^2}\left(\frac{\partial \mu_a}{\partial \lambda}\right)^2 + \frac{\partial A}{\partial \mu_s}\frac{\partial^2 \mu_s}{\partial \lambda^2} + \frac{\partial^2 A}{\partial {\mu_s}^2}\left(\frac{\partial \mu_s}{\partial \lambda}\right)^2 \tag{3}$$

Note that the independent variables within A now left out for clarity of presentation. Eq. 3 is 2nd differential expressions of attenuation with respect to wavelength respectively. It has been found that, with the chromophores present in tissue and with the weak wavelength dependence of scattering coefficient of tissue, the last three terms are small compared to the first term. If these terms are neglected, it gives the equation:

$$\frac{\partial^2 A}{\partial \lambda^2} \approx \frac{\partial A}{\partial \mu_a}\frac{\partial^2 \mu_a}{\partial \lambda^2} \tag{4}$$

However, now this equation has been derived without any assumption that A is linear with respect to $\mu_a(\lambda)$. Recall that the absorption coefficient is determined by the makeup of the chromophores (Eq. 5), (N_c : number of chromophores)

$$\mu_a = \sum_{i=1}^{Nc}(C_i \varepsilon_i) \tag{5}$$

So if the second-differential of absorption coefficient is determined by Eq. 6:

$$\frac{\partial^2 \mu_a}{\partial \lambda^2} = \sum_{i=1}^{Nc}\left(C_i \frac{\partial^2 \varepsilon_i}{\partial \lambda^2}\right) \tag{6}$$

Substituting Eq. 6 into Eq. 5, it yields:

$$\frac{\partial^2 A}{\partial \lambda^2} = \sum_{i=1}^{Nc}\left(\frac{\partial A}{\partial \mu_a}\cdot C_i \frac{\partial^2 \varepsilon_i}{\partial \lambda^2}\right) \tag{7}$$

Replacing $\partial A / \partial \mu_a$ with the label DP , we get below:

$$\frac{\partial^2 A}{\partial \lambda^2} = \sum_{i=1}^{Nc}\left(DP \cdot C_i \frac{\partial^2 \varepsilon_i}{\partial \lambda^2}\right) \tag{8}$$

If we discretize it into a certain wavelength range λ_i ($i = 1, \cdots, n$), we could get a matrix form:

$$\begin{bmatrix} \frac{\partial^2 A}{\partial \lambda^2}(\lambda_1) \\ \vdots \\ \frac{\partial^2 A}{\partial \lambda^2}(\lambda_n) \end{bmatrix} = \begin{bmatrix} DP(\lambda_1)\cdot\frac{\partial^2 \varepsilon_1}{\partial \lambda^2}(\lambda_1) & \cdots & DP(\lambda_1)\cdot\frac{\partial^2 \varepsilon_{Nc}}{\partial \lambda^2}(\lambda_1) \\ \vdots & \ddots & \vdots \\ DP(\lambda_n)\cdot\frac{\partial^2 \varepsilon_1}{\partial \lambda^2}(\lambda_n) & \cdots & DP(\lambda_n)\cdot\frac{\partial^2 \varepsilon_{Nc}}{\partial \lambda^2}(\lambda_n) \end{bmatrix} \cdot \begin{bmatrix} C_1 \\ \vdots \\ C_{Nc} \end{bmatrix} \tag{9}$$

The vector on the left side is the second-differential attenuation spectrum in this wavelength range which can be calculated from the attenuation spectrum measurement, the n-by- N_c matrix on the right side is the second-differential extinction coefficients spectra weighted by DP and the right side vector is the unknown chromophore concentrations. In figure 1, we plot the theoretical DP with respect to wavelength λ in a practical setup. Obviously, because the DP is wavelength-dependent, it seems this problem cannot be solved for either DP or C. To simplify the problem, we make the approximation that $DP(\lambda)$ is constant over a small wavelength range and use a single value, $\overline{DP}$, to represent $DP(\lambda)$ in this wavelength range, so that Eq. 9 can be transformed to:

$$\begin{bmatrix} \frac{\partial^2 A}{\partial \lambda^2}(\lambda_1) \\ \vdots \\ \frac{\partial^2 A}{\partial \lambda^2}(\lambda_n) \end{bmatrix} = \begin{bmatrix} \frac{\partial^2 \varepsilon_1}{\partial \lambda^2}(\lambda_1) & \cdots & \frac{\partial^2 \varepsilon_{Nc}}{\partial \lambda^2}(\lambda_1) \\ \vdots & \ddots & \vdots \\ \frac{\partial^2 \varepsilon_1}{\partial \lambda^2}(\lambda_n) & \cdots & \frac{\partial^2 \varepsilon_{Nc}}{\partial \lambda^2}(\lambda_n) \end{bmatrix} \cdot \overline{DP} \cdot \begin{bmatrix} C_1 \\ \vdots \\ C_{Nc} \end{bmatrix} \tag{10}$$

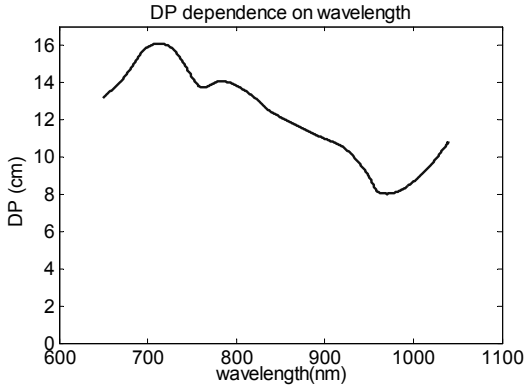

Figure 1, Differential pathlength dependence as a function of wavelength is shown for a simulation of light transport across a rat head. The variation with wavelength illustrates the need to quantify this value at all possible wavelength.

This approximation is quite reasonable and accurate when the variation of DP in this wavelength range is small or the second-differential extinction coefficient spectrum has a significant feature at certain wavelength. Now, the right side matrix turns to the second differential extinction coefficient spectra which are well known. Applying multilinear regression method, we can obtain $\overline{DP}$ scaled concentrations, $\overline{DP} \cdot C_i$ ($i = 1, \cdots, N_c$). Since one of the important chromophores, water, can be measured by other technologies accurately (i.e., the water concentration C_w is well known) $\overline{DP}$ can be extracted out from $\overline{DP} \cdot C_w$. Consequently other chromophore concentrations could also be derived. We define this estimate of $\overline{DP}$ as DPW, which is the differential pathlength at the wavelength of a water peak.

[18] Examining the second differential spectrum of the water extinction coefficient, three significant features exist in the near infrared range, respectively near 720nm, 820nm and 950nm. In our full spectral system, we choose ranges 700-800nm and 800-880nm to fit based on Eq. 9. Therefore, DPW around 720nm and 820nm can be estimated. Figure 1 tells us the wavelength dependence of DP in 800-880nm range is relatively small, therefore we expect this estimated DPW would be quite similar to the actual DP around 820nm. However, the estimated DPW in 700-800nm range is expected to be different to the actual DP around 720nm, since the relation between DP and wavelength is more complex in this range and there is a large hemoglobin (Hb) feature in the second differential extinction coefficient spectrum that would bring some crosstalk to the multilinear regression and lead to poor estimate of DPW. To test our hypotheses, we perform a series of experiments simulated by our FEM forward problem solver which is based on diffusion approximation. Measurements for both full spectral system and frequency domain system will be generated by this forward solver and DPW will be calculated using full spectral system method then compared with the actual DP predicted by the phase shift in frequency domain system. There are many reasons that lead us to choose a FEM forward solver to simulate data. Since our ultimate goal is to use FEM inverse problem solver to help us reconstruct images in full spectral system and both the FEM forward and inverse solvers have been proved to be effective in many applications, using FEM forward solver to perform experiments not only makes it easier to compare full spectral system and frequency domain system but also gives us a well controlled environment.

2.2Estimate of the differential pathlength in a heterogeneous medium

The previous discussion was limited to a homogeneous medium. In a more practical situation, one could divide the object into small nodes. [4, 24] Each node has its partial differential pathlength ($PDP_j = \partial A / \partial \mu_{a,j}$) and makeup of chromophores ($C_{i,j}$). Here $i = 1, \cdots, N_c$; $j = 1, \cdots, N_n$ (N_n : number of nodes).

$$DP = \sum_{j=1}^{Nn} PDP_j \tag{11}$$

The summation of partial differential pathlength is believed to be the differential pathlength. Eq. 4 therefore should be changed to:

$$\frac{\partial^2 A}{\partial \lambda^2} \approx \sum_{j=1}^{Nn} \left(\frac{\partial A}{\partial \mu_{a,j}} \cdot \frac{\partial^2 \mu_{a,j}}{\partial \lambda^2} \right) \tag{12}$$

And Eq. 7 and Eq. 8 now become:

$$\frac{\partial^2 A}{\partial \lambda^2} = \sum_{j=1}^{Nn} \left[\frac{\partial A}{\partial \mu_{a,j}} \cdot \left(\sum_{i=1}^{Nc} C_{i,j} \frac{\partial^2 \varepsilon_i}{\partial \lambda^2} \right) \right] \tag{13}$$

$$\frac{\partial^2 A}{\partial \lambda^2} = \sum_{j=1}^{Nn} \left[PDP_j \cdot \sum_{i=1}^{Nc} \left(C_{i,j} \frac{\partial^2 \varepsilon_i}{\partial \lambda^2} \right) \right] \tag{14}$$

If we use the same fitting method and assumptions made above, the value of $\sum_{j=1}^{Nn} (\overline{PDP}_j \cdot C_{w,j})$ can still be estimated. The value from the measurements is the summation of water concentration weighted partial differential pathlength, if we keep using the average water concentration.

$$DPW = \frac{\sum_{j=1}^{Nn} (\overline{PDP}_j \cdot C_{w,j})}{\frac{1}{N_n} \sum_{j=1}^{Nn} C_{w,j}} \tag{15}$$

[4] Obviously, this approximation will deviate far from the true value when the water heterogeneity is remarkable as people have shown. Therefore, we cannot get very accurate DP estimate directly from the measurement unless the water concentration distribution is homogeneous over all the sub regions. In this paper, we also will carry out some experiments on the water heterogeneous phantom to show such deviation if using Eq. 15.

2.3 Estimate the differential pathlength using sensitivity function weighted water concentration

In reality, we are always faced with heterogeneous situations. [4]No matter the case of arm measurements or our case of brain measurements, tissues are layered as skin, muscle, bone and regions due to pathologies. Each layer has different water concentrations. To take this effect upon the DP estimate into account, we want to introduce one possible solution. First, using the definition of DP, differential pathlength is the change of attenuation resulted from a small change of μ_a ($\partial A / \partial \mu_{a,j}$). [25] In frequency domain system, there is a very similar term called the sensitivity function (also called the Jacobin matrix, see Eq. 16) which relates the change in the boundary data (either intensity I or phase θ) with respect to a small change in either μ_a or κ (diffusion coefficient). The sensitivity between log of intensity and μ_a is part of the sensitivity function. (M: number of measurements)

$$J = \left| \begin{array}{cccc;{2pt/2pt}cccc}
\frac{\delta \ln I_1}{\delta \kappa_1} & \frac{\delta \ln I_1}{\delta \kappa_2} & \cdots & \frac{\delta \ln I_1}{\delta \kappa_{Nn}} & \frac{\delta \ln I_1}{\delta \mu_{a1}} & \frac{\delta \ln I_1}{\delta \mu_{a2}} & \cdots & \frac{\delta \ln I_1}{\delta \mu_{aNn}} \\
\frac{\delta \theta_1}{\delta \kappa_1} & \frac{\delta \theta_1}{\delta \kappa_2} & \cdots & \frac{\delta \theta_1}{\delta \kappa_{Nn}} & \frac{\delta \theta_1}{\delta \mu_{a1}} & \frac{\delta \theta_1}{\delta \mu_{a2}} & \cdots & \frac{\delta \theta_1}{\delta \mu_{aNn}} \\
\frac{\delta \ln I_2}{\delta \kappa_1} & \frac{\delta \ln I_2}{\delta \kappa_2} & \cdots & \frac{\delta \ln I_2}{\delta \kappa_{Nn}} & \frac{\delta \ln I_2}{\delta \mu_{a1}} & \frac{\delta \ln I_2}{\delta \mu_{a2}} & \cdots & \frac{\delta \ln I_2}{\delta \mu_{aNn}} \\
\frac{\delta \theta_2}{\delta \kappa_1} & \frac{\delta \theta_2}{\delta \kappa_2} & \cdots & \frac{\delta \theta_2}{\delta \kappa_{Nn}} & \frac{\delta \theta_2}{\delta \mu_{a1}} & \frac{\delta \theta_2}{\delta \mu_{a2}} & \cdots & \frac{\delta \theta_2}{\delta \mu_{aNn}} \\
\vdots & \vdots & \ddots & \vdots & \vdots & \vdots & \ddots & \vdots \\
\frac{\delta \ln I_M}{\delta \kappa_1} & \frac{\delta \ln I_M}{\delta \kappa_2} & \cdots & \frac{\delta \ln I_M}{\delta \kappa_{Nn}} & \frac{\delta \ln I_M}{\delta \mu_{a1}} & \frac{\delta \ln I_M}{\delta \mu_{a2}} & \cdots & \frac{\delta \ln I_M}{\delta \mu_{aNn}} \\
\frac{\delta \theta_M}{\delta \kappa_1} & \frac{\delta \theta_M}{\delta \kappa_2} & \cdots & \frac{\delta \theta_M}{\delta \kappa_{Nn}} & \frac{\delta \theta_M}{\delta \mu_{a1}} & \frac{\delta \theta_M}{\delta \mu_{a2}} & \cdots & \frac{\delta \theta_M}{\delta \mu_{aNn}}
\end{array} \right| \tag{16}$$

Clearly $\frac{\delta \ln I}{\delta \mu_{a,j}}$ is equal to $-\frac{\partial A}{\partial \mu_{a,j}}$ since the attenuation is the difference of log of intensity between at detector and at source. Therefore the partial differential pathlength should be modeled by the nodal sensitivity function. If we sum the sensitivity at all nodes, we should get the DP:

$$DP = \sum_{j=1}^{Nn} PDP_j = -\sum_{j=1}^{Nn} \frac{\delta \ln I}{\delta \mu_{a,j}} \tag{17}$$

In this paper, we will calculate the Jacobin matrix with our FEM solver and compare the DP calculated by Eq. 17 with the DP calculated from phase shift measurement to examine this conclusion. (We named this DP derived from Jacobin matrix as DPJ.)

Instead of using average water concentration to estimate DP in Eq. 15, we will use a new term to compensate the water inhomogeneity.

$$\overline{C}_w = \frac{\sum_{j=1}^{Nn} \left(\frac{\delta \ln I}{\delta \mu_{a,j}} \cdot C_{w,j}\right)}{\sum_{j=1}^{Nn} \frac{\delta \ln I}{\delta \mu_{a,j}}} \tag{18}$$

This term is sensitivity weighted mean water concentration. Here, $C_{w,j}$ is the water concentration map we could get from MRI. $\frac{\delta \ln I}{\delta \mu_{a,j}}$ is the sensitivity function we could calculate based on our initial guess of optical properties. [20, 21]This initial guess also could utilize a priori information endowed by MRI. Then we could modify Eq. 15 with this new term $\overline{C}_w$.

$$DPW = \frac{\sum_{j=1}^{Nn} \left(\overline{PDP}_j \cdot C_{w,j}\right)}{\overline{C}_w} = \frac{\sum_{j=1}^{Nn} \left(\overline{PDP}_j \cdot C_{w,j}\right) \cdot \sum_{j=1}^{Nn} \frac{\delta \ln I}{\delta \mu_{a,j}}}{\sum_{j=1}^{Nn} \left(\frac{\delta \ln I}{\delta \mu_{a,j}} \cdot C_{w,j}\right)} \tag{19}$$

Clearly, if we could iteratively update the modeled optical properties in FEM until they match the true value, the denominator in the above equation will be canceled by the first term in the numerator which is the value obtained by full spectral system. The remaining equation becomes:

$$DP = -\sum_{j=1}^{Nn} \frac{\delta \ln I}{\delta \mu_{a,j}^*} \tag{20}$$

This is the accurate solution of DP. At the same time, we also get the optimal solution of optical properties ($\delta \mu_{a,j}^*$).

Therefore, an iterative algorithm is needed to make the model converge to the true value. In the first step, the intensity measurement (I) and water weighted differential pathlength ($\sum_{j=1}^{Nn} \left(\overline{PDP}_j \cdot C_{w,j}\right)$) could be measured from full spectral system. With the water map and initial guess of optical property maps, we could use Eq. 19 to calculate an estimate of DP. Then we convert this estimate (DPW) into a phase estimate ($\tilde{\theta}$). Comparing $\tilde{\theta}$ and the intensity measurement I with model calculated $\theta_{\mathrm{mod}el}$ and $I_{\mathrm{mod}el}$, we can use the difference to update optical properties μ_a or κ. Finally, going back to use Eq. 19 again to calculate DPW. This is iteratively repeated until the problem converges, and finally the optical properties maps are obtained.

3. EXPERIMENTS AND RESULTS

3.1 Comparison of DPW and DPP in homogenous phantom

Since the experiment data is simulated by the FEM forward solver, we need to define the geometry, source and detector positions and create mesh for it. In the first series of experiments, we will focus on homogenous phantoms. Figure 2 shows the mesh of a homogenous phantom and one source and 8 detectors are drawn as star and circles respectively on the mesh. The diameter of this circular phantom is 30mm and meshed with 1785 nodes. The makeup of the phantom is oxy-hemoglobin (HbO), deoxy-hemoglobin (Hb), water and intralipid and the concentrations of these components are chosen in the range similar to the values typical of rat brain. [26, 27]Since the optical properties of these components have been measured (Optical properties paper), we calculated the absorption coefficient spectrum $\mu_a(\lambda)$ using Eq. 5 and the extinction coefficient spectra of Hb, HbO and water and we also calculated the scattering coefficient spectrum $\mu'_s(\lambda)$ by assuming all the scattering is caused by intralipid. Based on these optical properties ($\mu_a(\lambda)$, $\mu'_s(\lambda)$), the intensity spectrum $I(\lambda)$ and phase shift spectrum $\theta(\lambda)$ for each source detector pairs were calculated by FEM forward solver at each wavelength from 650nm to 1040nm with interval of 1/3nm. Then use the intensity spectrum to yield the simulated attenuation spectrum $A(\lambda)$ for full spectral system. We fit every 40nm width attenuation spectrum to a 3-order polynomial, so that the second differential value at the midpoint of this sliding window was calculated. Because the wavelength is even sampled, we could convert such fitting algorithm to convolute with a fixed matrix, therefore the speed of calculation was very fast. This method is also a smoothing process which could weaken the influence of noise to the second differential spectrum. Next we calculated DPW around 720nm and 820nm using the method discussed in the first part of method section. Finally, we compared these two DPW with the DP calculated from the phase shift at 720nm and 820nm for different phantom setup. Moreover, noise was added to test the robustness of the algorithm.

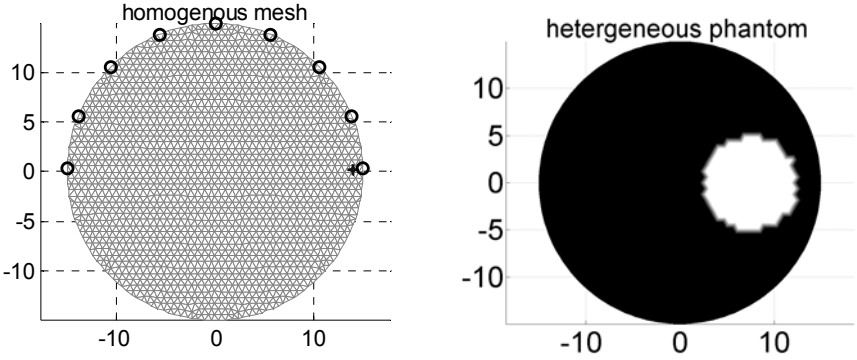

Figure 2, (a) Left: mesh of homogeneous phantom. The detector positions are shown by small circles. The source position is shown by a cross. (b) Right, the heterogeneous phantom

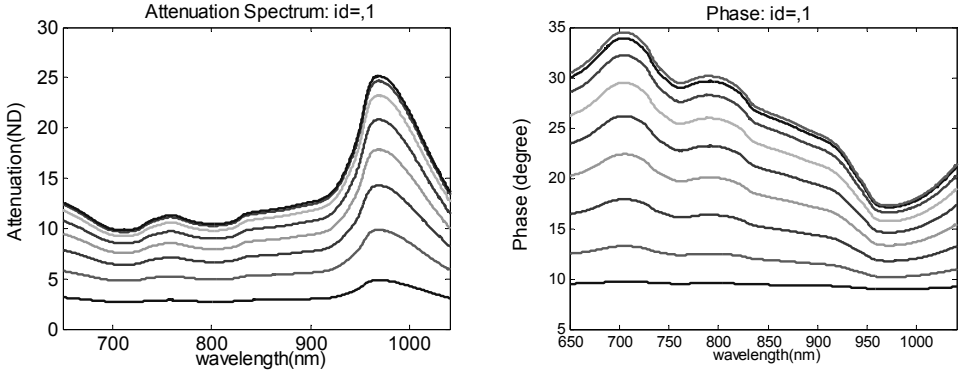

Figure 3, (a) Left, simulated attenuation spectra at all detectors, (b) Right, simulated phase spectra at all detectors. (For experiment 1)

Index	*Ct (uM)*	*Sa (%)*	*Water (%)*	*Intralipid (%)*
1	**120**	**70**	**85**	**1**
2	**100**	**70**	**85**	**1**
3	**120**	**65**	**85**	**1**
4	**120**	**70**	**80**	**1**
5	**120**	**65**	**80**	**1**

Table 1. Simulation experiment setups for the homogeneous phantom. Here *Ct* is the total hemoglobin concentration. *Sa* is the oxygen saturation.

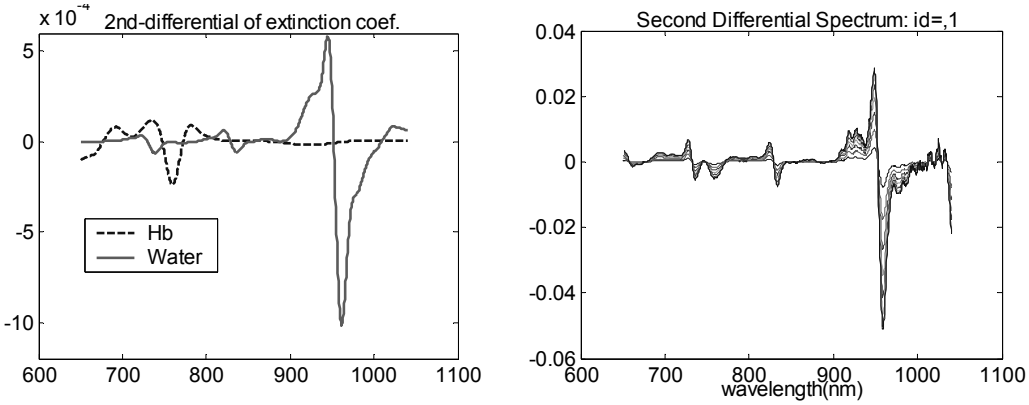

Figure 4, (a) Left: second differential spectra of extinction coefficients (weighted by concentrations), (b) Right: second differential spectra at all detectors (for experiment 1)

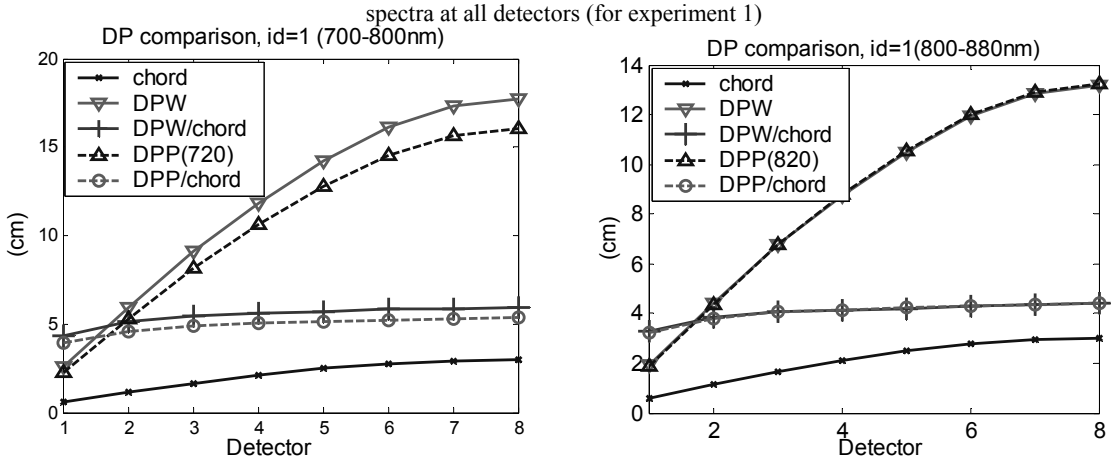

Figure 5, (a) Left: Comparison of DP estimated by water peak (DPW), DP calculated by phase shift (DPP) and Physical Distance (chord) at 720nm feature, (b) Right: of DPW, DPP, and optode separation at 820nm feature.

Table 1 lists the setups of 5 homogeneous experiments, index from 1 to 5. C_t is the concentration of total hemoglobin. Sa is the oxygen saturation. The 1st experiment is the start point. The 2nd to 4th were experiments with changing only C_t, Sa, Water respectively. The 5th was changing those three together. Figure 3 shows the attenuation spectrum and phase shift spectrum calculated by the FEM forward solver at all detectors (different lines) for experiment 1. Detector 1 is the nearest one and Detector 8 is the opposite one to the source. Figure 4 shows the second differential spectra of extinction coefficients (a) and attenuation (b) respectively. Figure 5 (a) shows the comparison of DPW, DPP, optode separation (chord) and differential pathlength factor (DPF = DP/chord) at all the detectors for fitting in 700-800nm range. Figure 5(b) is the same as the Figure 5 (a) instead for 800-880nm range. We can see that the differential pathlength estimated using water features is very close to that calculated from the phase shift for the 820nm water feature, while not for the 720nm water feature. This result agreed with our hypotheses made in the previous section. The same procedure is performed on all the phantoms listed in Table 1. The mean and standard deviation (STD) of the difference between DPW and DPP were analyzed and summarized in Table 2 for all these experiments. We found that the difference at 820nm was very small (less than 1%) and consistent with different detector positions, however, the difference at 720nm was large. This encouraging finding proved our assumption that the differential pathlength estimated in full spectral system is equivalent to the phase shift measurement in frequency domain system at least for homogeneous phantom and implied it's possible to reconstruct an image using FEM inverse solver.

We applied second differential analysis during our process, so it implied noise may have a big impact on the second differential spectrum. To test the effectiveness of noise reduction in our algorithm, we added 0.1% of Gaussian distributed random noise into the attenuation spectrum. Although the mean difference between DPW and DPP did increase for a single measurement, it dropped significantly when we averaged 20 measurements. The comparison is shown in Table 3. Averaging is a very common process we use in reality, therefore the noise issue should not be an obstacle to precede this

approach.

	Difference of DP (720nm)		*Difference of DP (820nm)*	
Index	***Mean (%)***	***STD***	***Mean (%)***	***Std***
1	**11.12**	**0.0032**	**0.52**	**0.0056**
2	**8.66**	**0.0032**	**0.82**	**0.0035**
3	**10.8**	**0.0032**	**0.52**	**0.0060**
4	**11.9**	**0.0031**	**0.51**	**0.0061**
5	**9.08**	**0.0031**	**0.75**	**0.0037**

Table 2, Statistical estimates from the experimental results, showing mean and standard deviation values.

	Difference of DP (820nm) (%)	
	Mean (%)	***Std***
Single measurement	**3.27**	**0.0566**
Average of 20	**0.81**	**0.0039**

Table 3, Estimates of the noise impact upon the esmation of Differential Pathlength (DP) and the reduction in the error that can be achieved by averaging of 20 measurements.

3.2 Comparison of DPWand DPP in heterogeneous phantom

Beyond the homogeneous model, we did the same procedure for a series of heterogeneous phantom, either the total Hb heterogeneous phantom or water heterogeneous phantoms. In Figure 2 (b), we show the geometry of the heterogeneous phantom. A circular region with 5mm radius is added at the midpoint between center and boundary. 5 experiments were carried out. First one is the homogeneous phantom as our initial setup. In second experiment, we doubled the total Hb (C_t) concentration of the circular region. In the next three experiments, we decreased the water concentration in the circular region by 5% per experiment. The DPW was calculated using Eq. 15. We plot the difference between DPW and DPP of 820nm at all detector positions for all these 5 experiments in Figure 6. Clearly increase of water heterogeneity would also increase the difference between DPW and DPP. We also observed an increase in the case that C_t was doubled, however this increased difference was relatively small compared to the actual DP changes when doubled C_t, while not for the water heterogeneous cases. Moreover, 5% water heterogeneity led to the similar error as 100% C_t heterogeneity. Therefore, the water heterogeneity would be more critical to our mapping from DPW to DPP.

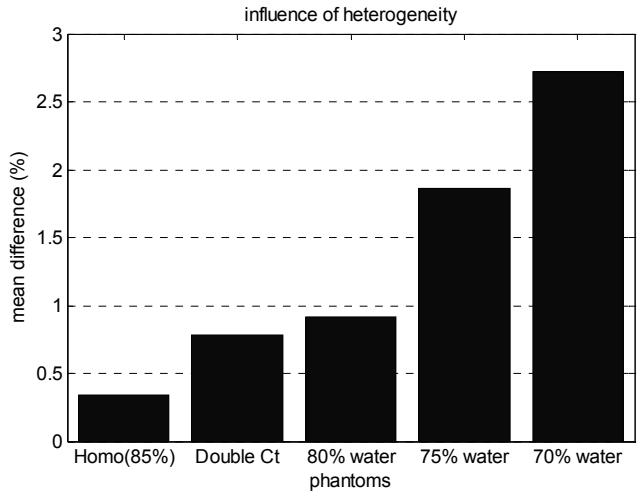

Figure 6, Illustration of the influence of heterogeneity upon the mean difference between DPW and DPP when varying the total hemoglobin concentration (C_t) or water concentration of a circular region in the homogeneous phantom. The background C_t was 100μM and water was 85%. 1st: homogeneous case, 2nd: doubled C_t = 200μM, 3rd: 80% water, 4th: 75%, 5th: 70%.

3.3 Comparison of DP derived from sensitivity function andDPP

Further, we performed some experiments to compare the relationship between the sensitivity function (log intensity to μ_a) and DP calculated from phase shift to examine our guess made in Eq. 19. We tested three phantoms. Phantom 1 is a homogeneous phantom as shown in Figure 1 with $\mu_a = 0.01mm^{-1}$ and $\mu_s^{'} = 1.0mm^{-1}$. Phantom 2 is added a circular

region (shown in Figure 7(a)) ($\mu_a = 0.02mm^{-1}$) to the Phantom 1. Phantom3 is added three circular regions (shown in Figure 7(b)). The right top region: $\mu_a = 0.02mm^{-1}$; the bottom region: $\mu_a = 0.03mm^{-1}$; the left top region: $\mu_s' = 1.5mm^{-1}$. Here, we defined the DP calculated by Eq. 16 from Jacobin matrix as DPJ. In Figure 8, we compared DPJ and DPP for these three phantoms and we also plotted the identical line to demonstrate how DPJ agreed with DPP. We used 1st polynomial to fit the relationship between DPJ and DPP, and we found the slope was less than 1.0001 for all the phantoms. Therefore, the DP derived from the sensitivity function (Jacobin matrix) is equivalent to the DP calculated from phase shift. This important discovery would make the strategy we discussed in previous section possible.

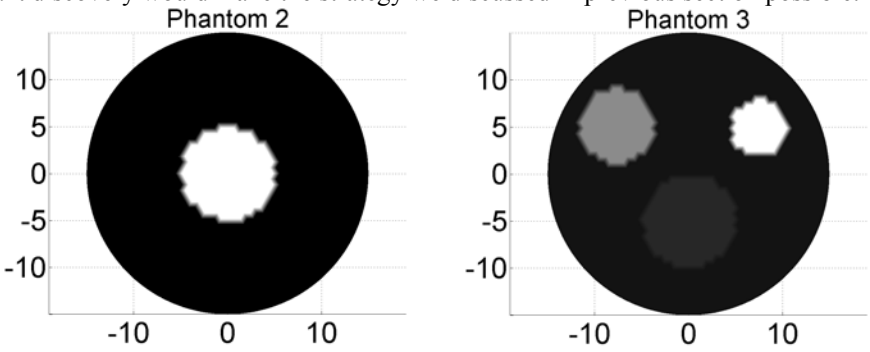

Figure 7, (a) Left: Phantom 2, a circular region: $\mu_a = 0.02mm^{-1}$, (b) Right: Phantom 3, the right top region: $\mu_a = 0.02mm^{-1}$; the bottom region: $\mu_a = 0.03mm^{-1}$; the left top region: $\mu_s' = 1.5mm^{-1}$. Background: $\mu_a = 0.01mm^{-1}$ and $\mu_s' = 1.0mm^{-1}$

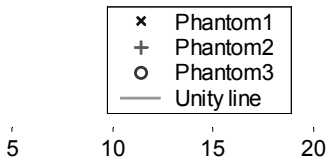

Figure 8, DPP (DP calculated from phase shift) vs. DPJ (DP calculated by summing Jacobin matrix) for phantoms 1, 2, 3, showing the linear agreement between the two estimates of differential pathlength.

4. DISCUSSION

We want to further our discussion based on the simulation results. In the first series of experiments, we showed our success to match DP estimated from water feature in full spectral system to the DP calculated from phase shift measurements in the frequency domain system. We also demonstrated that the wavelength range chosen to fit data affected the estimates greatly. The estimate from the 800-880nm range is more accurate than that of the 700-800nm range. This discrepancy was expected from our supposition made in the methods section. In the 700-800nm range, there is a large second-differential feature of deoxy-hemoglobin which generates some crosstalk in water feature and the noticeable wavelength-dependence of DP deteriorates the estimate, while this doesn't happen in the 800-880nm range and therefore we could get an accurate estimate of DP around the water feature.

In our simulations, we also considered more practical situations. We added some noise to the attenuation measurements to simulate the environment we faced with in full spectral system. Although the estimate was greatly influenced by the noise, we were still able to almost eliminate it by simple signal processing.

In the second series of experiments, we demonstrated the impacts of heterogeneity. The results agreed with our expectations discussed in the methods section. It proved that the water heterogeneity would be the most significant factor to our mapping from DPW to DPP. Although we also saw the deviation with increasing hemoglobin concentration, it does not appear to be a critical problem, since the variation of DP with double total hemoglobin is also very large. Moreover, if we just made smaller changes of Ct instead of doubling, much smaller deviation would be observed.

In the last series of experiments, we furthered our study into the relationship between the sensitivity function and the DP. We have verified that the summation of $\frac{\delta \ln I}{\delta \mu_{a,j}}$ in the sensitivity function is equivalent to the DP independent of the phantom used. This strengthens our confidence that the iterative method to reconstruct images with the CCD full spectral system will be successful.

5. CONCLUSIONS

In this paper, we found that the differential pathlength estimated in the spectroscopy system was almost equivalent to the phase shift measurement in frequency domain system for water homogeneous phantoms. For water heterogeneous cases, we also proposed a possible solution with testing some fundamental problems. We believe that we could map the measurements of CCD full spectral system into frequency domain system. Therefore, we would be able to utilize the finite element method solver to reconstruct tomographic images in the CCD full spectral system. If these development bear out to be true in experiments, this approach will provide the first viable method to reconstruct images of absorption and scattering coefficient from measurements of continuous wave spectral data.

6. ACKNOWLEDGEMENTS

This work has been supported by the National Institute of Health through grants NIH RO1 NS38471 and RO1 CA69544.

7. REFERENCES

1. Jobsis, F.F., *Non-invasive, infra-red monitoring of cerebral and myochardial oxygen sufficiency and circulatory parameters.* Science, 1977. **198**: p. 1264-1267.
2. Brazy, J.E., et al., *Noninvasive monitoring of cerebral oxygenation in preterm infants: preliminary observations.* Pediatrics, 1985. **75**(2): p. 217-25.
3. Cope, M., Van der Zee, P., Essenpreis, M., Arridge, S. R., Delpy, D. T., *Data analysis methods for near infrared spectroscopy of tissue: problems in determining the relative cytochrome aa3 concentration.* SPIE Time-Resolved Spectroscopy and Imaging of Tisssues, 1991. **1431**: p. 251-262.
4. Matcher, S.J., Cope, M. , Delpy, D. T., *Use of the water absorption spectrum to quantify tissue chromophore concentration changes in near-infrared spectroscopy.* Phys. Med. Biol., 1993. **38**: p. 177-196.
5. Cope, M., et al., *A CCD spectrophotometer to quantitate the concentration of chromophores in living tissue utilising the absorption peak of water at 975 nm.* Adv Exp Med Biol, 1989. **248**: p. 33-40.
6. Cooper, C.E., Elwell, C. E., Meek, J. H., Matcher S. J., Wyatt, J. S., Cope, M., Delpy, D. T., *The noninvasive measurement of absolute cerebral deoxyhaemoglobin concentration and mean optical pathlength in the neonatal brain by second derivative near infrared spectroscopy.* Pediat. Res., 1996. **39**: p. 32-38.
7. Delpy, D.T., Cope, M., Van der Zee, P., Arridge, S. R., Wray, S., Wyatt, J.S., *Estimation of optical pathlength though tissue from direct time of flight measurement.* Phys. Med. Biol., 1988. **33**: p. 1433-1442.
8. Delpy, D.T., et al., *Quantitation of pathlength in optical spectroscopy.* Adv Exp Med Biol, 1989. **248**: p. 41-6.
9. Chance, B., *Near-infrared images using continuous, phase-modulated, and pulsed light with quantitation of blood and blood oxygenation.* Annals of the New York Academy of Sciences, 1998. **838**: p. 29-45.
10. Chance, B., Maris M, Sorge, J. and Zhang, M. Z., *A phase modulation system for dual wavelength difference spectroscopy of haemoglobin deoxygenation in tissue.* Proc. SPIE, 1990. **1204**: p. 481-91.
11. Patterson, M.S., Moulton, J. D., Wilson, B. C. and Chance, B., *Applications of time resolved light scattering measurements to photodynamic therapy dosimetry.* Proc. SPIE, 1990. **1431**(84-96).

12. Arridge, S.R., Cope, M., Delpy, D. T., *The theoretical basis for the determination of optical pathlengths in tissue: temporal and frequency analysis.* Phys. Med. Biol., 1992. **37**(7): p. 1531-1560.
13. Paulsen, K.D., and Jiang H., *Spatially varying optical property reconstruction using a finite element diffusion equation approximation.* Med. Phys., 1995. **22**(6): p. 691-701.
14. Paulsen, K.D., Jiang, H., *Enhanced frequency-domain optical image reconstruction in tissues through total-variation minimization.* Appl. Opt., 1996. **35**(19): p. 3447-3458.
15. Arridge, S.R., et al., *A finite element approach for modeling photon transport in tissue.* Med Phys, 1993. **20**(2 Pt 1): p. 299-309.
16. Kaltenbach, J.M., Kaschke, M., *Frequency and time-domain modelling of light transport in random media*, in *Medical Optical Tomography: Functional Imaging and Monitoring*, G. Muller, Editor. 1993, SPIE Publ.: Bellingham, WA.
17. Pogue, B.W., *Frequency-domain optical spectroscopy and imaging of tissue and tissue-simulating media.*, in *Physics Dept.* 1996, McMaster University: Hamilton Canada.
18. Matcher, S.J., Cooper, C. E., *Absolute quantification of deoxyhaemoglobin concentration in tissue near infrared spectroscopy.* Phys. Med. Biol., 1994. **39**: p. 1295-1312.
19. McBride, T.O., et al., *Initial studies of in vivo absorbing and scattering heterogeneity in near-infrared tomographic breast imaging.* Opt. Lett., 2001. **26**(11): p. 822-824.
20. Pogue, B.W., T. O. McBride, C. Nwaigwe, U. L. Osterberg, J. F. Dunn, K. D. Paulsen, *Near-infrared diffuse tomography with apriori MRI structural information: testing a hybrid image reconstruction methodology with functional imaging of the rat cranium.* Proc. SPIE, 1999. **3597**: p. 484-492.
21. Xu, H., Dehghani, H., Pogue, B. W., Springett, R., Paulsen, K. D., Dunn, J. F., *Near-infrared imaging in the small animal brain: optimization of fiber positions. J. Biomed. Opt.*, 2003. **8**(1): p. 102-110.
22. Matcher, S.J., et al., *Performance comparison of several published tissue near-infrared spectroscopy algorithms.* Anal Biochem, 1995. **227**(1): p. 54-68.
23. Kohl, M., et al., *Determination of the wavelength dependence of the differential pathlength factor from near-infrared pulse signals.* Phys Med Biol, 1998. **43**(6): p. 1771-82.
24. Hiraoka, M., et al., *A Monte Carlo investigation of optical pathlength in inhomogeneous tissue and its application to near-infrared spectroscopy.* Phys Med Biol, 1993. **38**(12): p. 1859-76.
25. Arridge, S.R., Schweiger, M., *Sensitivity to prior knowledge in optical tomographic resconstruction.* Proc. SPIE, 1995. **2389**: p. 378-388.
26. Hale, G.M., Querry, M. R., *Optical constants of water in the 200nm-200μm wavelength region. Appl. Opt.*, 1973. **12**: p. 555-563.
27. van Staveren, H.J., et al., *Light Scattering in Intralipil-10% in the wavelength range of 400-1100nm.* Applied Optics, 1991. **30**(31): p. 4507-4514.